340 GHz FMCW pulse-Doppler radar to characterize the dynamics of particle clouds

Tomas Bryllert, *Member, IEEE*, Marlene Bonmann, and Jan Stake, *Fellow, IEEE*

***Abstract*—In this work, a 340 GHz frequency-modulated continuous-wave (FMCW) pulse-Doppler radar is presented. The radar system is based on a transceiver module with ≈ 0 dBm output power and >30 GHz bandwidth. The digital radar waveform generation allows for coherent and arbitrary FMCW pulse waveforms. The performance in terms of sensitivity and resolution (range/cross-range/velocity) is demonstrated and the system's ability to detect and map single particles, as well as clouds of particles, at 5m distance, is presented. The antenna/optics consists of an off-axis parabola fed by a horn antenna from the transceiver unit, resulting in a collimated radar beam. A range resolution of ~1 cm and a cross-range resolution of a few centimeters (3 dB beam-width) allow for characterization of the dynamics of particle clouds with a measurement voxel size of a few cm^3.**

The monitoring of particle dynamics is of interest in several industrial applications, such as in the manufacturing of pharmaceuticals, and in the control/analysis of fluidized bed combustion reactors.

***Index Terms*—Radar, FMCW, pulse-Doppler, millimeter wave, THz**

I. Introduction

For many industrial applications, such as in the manufacturing of pharmaceuticals or in energy conversion using fluidized bed reactors, the industrial process involves particles or powders that are dispersed in a process reactor. It is necessary to monitor the particle/powder dynamics to maintain the process quality and to gain insights regarding the process. It is therefore desirable to be able to measure the particle concentration and the local particle velocities at high update rate and at high spatial resolution. Ideally, these quantities should be measured without inserting any physical probes into the reactors, so that the processes are not altered by the introduction of measurement sensors. It is also sometimes difficult to get physical access to the process reactors due to the harsh process environment. Frequency-modulated continuous-wave (FMCW) range-Doppler radar operating at center frequencies within the sub-millimeter wave range (300-1000 GHz) of the electromagnetic spectrum offer a realistic opportunity to provide the desired information. Compared to other contactless measurement methods (laser-based techniques) that are operating at optical frequencies (400-700 THz), the lower sub-millimeter wave frequencies allow larger penetration depth into dense particle clouds as well as being less sensitive to contaminations on the reactor access windows. The radar technique also allows for Doppler processing, which reveals information about the velocities the particles. Comparing with more traditional radar techniques at microwave/millimeter wave frequencies, there are a few properties that favor higher frequencies:

- The relatively high frequency results in a higher sensitivity for detection of smaller particles (the radar cross-section of particles in the Rayleigh regime scales as λ^{-4}).
- It is easier to achieve high bandwidth, and thereby a higher range resolution (30 GHz bandwidth results in a theoretical range resolution of 0.5 cm)
- The cross-range resolution, for a fixed antenna size (typically limited by the access window size in a real application) improves with high frequency (the diffraction limited resolution scales with λ).

Several FMCW radars for high-resolution 3-D radar imaging have been presented with center frequencies at ~340 GHz [Sheen2010, Cheng2018, Robertson2018, Cooper2011]. These systems use ranging to produce 3D static images and are not using pulse-Doppler processing. Cooper et al. [Cooper2014] reported a FMCW range-Doppler radar system at 660 GHz demonstrating the feasibility of the pulse-Doppler concept at submillimeter wave frequencies, but with few details.

In this work, the implementation of a FMCW pulse-Doppler radar based on a 340 GHz transceiver module with 30 GHz bandwidth [Dahlbäck2016] is presented The system is controlled by a digital waveform generator. The transceiver module provides an acceptable trade-off between performance and hardware complexity, resulting in a relatively compact tripod-mounted radar design (fig 2). The form-factor allow easy implementation in industrial scenarios.

The performance of the transceiver modules themselves, and their application in a 3D imaging radar, was presented in [Robertson2018]. Here the implementation of the coherent pulse generation and signal processing to realize range-Doppler radar operation are presented, together with the noise- and

To be submitted. This work was supported in part by "the Swedish Foundation for Strategic Research" under the contract ITM17-0265

Tomas Bryllert, Marlene Bonmann and Jan Stake are with the Department of Microtechnology and Nanoscience, Terahertz and Millimetre Wave Laboratory, Chalmers University of Technology, SE-412 96 Gothenburg,Sweden (email: tomas.bryllert@chalmers.se)

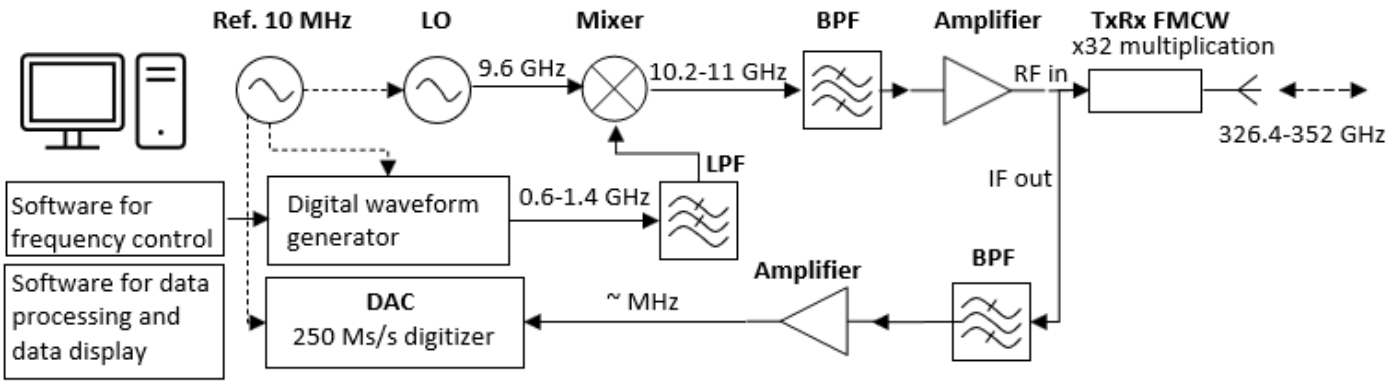

Fig. 1. Change figure A schematic block diagram of the submm-wave FMCW pulse-Doppler radar system. The system is fully coherent and the waveforms are generated from a digital waveform card. A dedicated TxRx fronted module translates the frequency from X-band to 340 GHz.

resolution-performance of the resulting radar system. Furthermore, the ability of the radar to detect single particles with diameters ranging from 75 μm-350 μm is demonstrated.

Fig. 2. Photograph of the radar system, ready to perform measurements in an industrial environment.

The accuracy of the velocity measurements are validated by comparing the measured range-Doppler profile of a falling metal bead with known weight and diameter to the theoretical free-fall model. The results demonstrate that the performance of the radar system is highly suitable for the suggested industrial experimental scenarios.

II. Radar Hardware

Figure 1 shows a schematic block diagram of the 340 GHz FMCW range-Doppler radar, the system architecture is a frequency up-converted, frequency multiplied FMCW radar.
A few hardware details deserves to be highlighted: The digital waveform generator is an FPGA controlled arbitrary waveform card with 4 Gb of useful memory and a maximum sampling rate of > 6Gs/s (4Gs/s is used in the current work). The card is capable of writing >100 ms of 1 GHz bandwidth waveform data directly from memory. This means that, in a typical coherent pulse-Doppler processing interval (CPI), which is typically (much) shorter than 100 ms, an arbitrary pulse train of FMCW pulses can be transmitted – and then repeated. This means that multiple FMCW waveforms can be interleaved addressing different parts of the system bandwidth (323 – 357 GHz) within a coherent processing interval. This capability can be used to extract frequency resolved (spectroscopic) information from the scene in an optimized way. This feature is not used in the presented performance demonstrations.
The baseband chirp (typically 1 GHz bandwidth), that is generated by the digital hardware, is centered at 1 GHz. This signal is up-converted to X-band using frequency mixing and a 9.6 GHz LO, and is then passed on to the transceiver unit. The transceiver unit multiplies the X-band chirp by a factor of 32 for a total final bandwidth of 32 GHz and transmits the signal, now centered at ~340 GHz. The radar echoes are received back in the transceiver and are mixed on the outgoing signal, straight down to baseband. The transceiver is described in detail in [Dahlbäck2016].
The digital hardware on the receiver side consists of an 8 channel, 250 Ms/s digitizer from National Instruments (1 channel is used). The digitizer is controlled by an FPGA which gives deterministic timing control. The digitizer card (PXIe format) integrates with a PC controller via a PXIe bus allowing for real-time signal processing and display. The waveform card, the digitizer and the local oscillator in the system run from a common 10 MHz reference resulting in a fully coherent system.

III. Digital Signal Processing

Typical radar parameters used in the experiments presented in this work are:

- Pulse bandwidth = 32 GHz
- Pulse time = 41 us
- Pulse repetition interval (PRI) = 102.4 us
- Nr of pulses coherently processed (nr of PRI) = 128
- Target distance 4 – 6 m

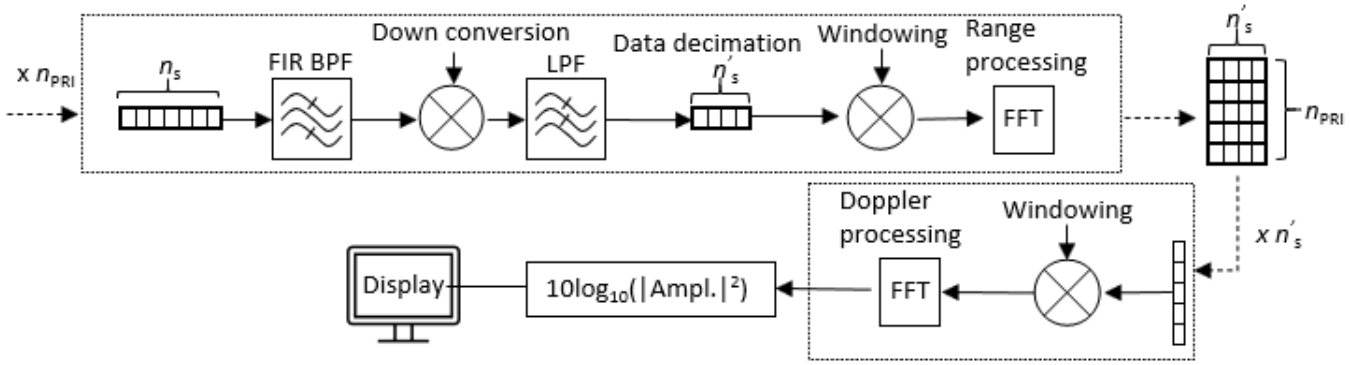

Fig. 3. Schematic block diagram of the digital signal processing steps.

The received baseband signal, after down-conversion in the transceiver is, with these parameters, in the range 21 – 31 MHz, which is digitized. The data is digitally filtered, converted to IQ format, down-converted to complex baseband and decimated to ~1.5 x Nyquist limited sampling (15.625 Ms/s IQ). The format of the data matrix that is coherently processed is then of the format:

- (nr of samples per pulse) x (nr of PRI)

with: nr of samples per pulse = 640, nr of PRI = 128.
In reality, a number of samples at the beginning and the end of each waveform are discarded (due to low frequency ringing), leaving 590 samples instead of 640. This also reduces the actual used bandwidth from 32 GHz to 29.5 GHz.
Both the pulse compression in range as well as the Doppler processing can be done using Fourier transforms in FMCW pulse-Doppler radar, which means that the signal processing is basically a 2D FFT over the coherent data matrix – with appropriate widowing functions and digital filters. Figure 3 shows a block diagram of the signal processing.

IV. System Evaluation - Measurements

To demonstrate the performance of the system in terms of noise floor, range/velocity resolution, small particle detection and validation of the measured velocity, the following measurements were conducted:

A. Noise performance

The noise floor in 0-Doppler and at finite Doppler frequency were investigated.

- The noise floor is measured for:
  - ADCs
  - ADCs with IF amplifiers
  - ADCs with IF amplifiers and a 10.1 GHz continuous wave (cw) signal driving the transceiver
  - ADCs with IF amplifiers and a chirp signal driving the transceiver (but no targets)
- The noise floor (both in 0-Doppler and at finite Doppler frequency) as a function of target strength is measured. Different radar cross sections (RCS) are achieved by placing a corner reflector at different positions in the radar beam.
- S/N as a function of number of coherent pulses in a processing interval

B. Range/Doppler resolution and small particle detection

To demonstrate the range resolution of the radar system, three metal beads with 1.5 mm diameter were glued onto a string and positioned at 5 m distance. A radar measurement was performed to demonstrate that the beads can be resolved. Gently tapping the string and making another radar measurement displays the Doppler sensitivity of the measurement.
To demonstrate the radar systems ability to detect small particles, the radar beam is folded with a flat metallic mirror to be directed vertically upwards. Directly above the folding-mirror a transparent plastic box was placed to collect the particles and metal spheres that are dropped straight down into the radar beam. The spheres and particles used were:

- 2 mm diameter metal beads
- 10 mm diameter metal beads (see section IV C)
- 500 um diameter particles of quartz sand

C. Validation of velocity measurement

The velocity measurement of the radar system was validated comparing the measured velocity of a free-falling metal sphere of known diameter (1.27 cm) and weight (8.44 g) with the theoretical free-fall model. Letting the metal bead drop towards the radar it moves vertically under the influence of gravity and air resistance. The velocity (v) and position (x) with time (t) is described by

- $v = \sqrt{mg/k}\ tanh(t\sqrt{gk/m})$
- $x = x_0 - m/k\ ln(cosh(t\sqrt{gk/m}))$

with k=0.5$\rho_{air}Ac_d$, where x_0 is the initial position, g is the gravity of Earth, m is the mass of the metal bead, $\rho_{air}$is the air density at normal temperature pressure, A is the metal beads cross section, and c_d is the drag coefficient (here 0.47 for a sphere).

V. System Evaluation – Results

A. *Noise performance*

Ideally, the noise floor in the whole range-Doppler map should be set by thermal noise, deteriorated by the loss and noise-figure of the frontend electronics and scaled by the IF amplification. The transceiver unit trades noise performance for simplicity though. By using the same balanced pair of Schottky diode circuits both for the final stage frequency multiplication and for subharmonic homodyne down-conversion to baseband [Dahlbäck2016], the transceiver unit can be made quite compact – at the cost of excess noise. The excess noise comes in two shapes – through a conversion-loss

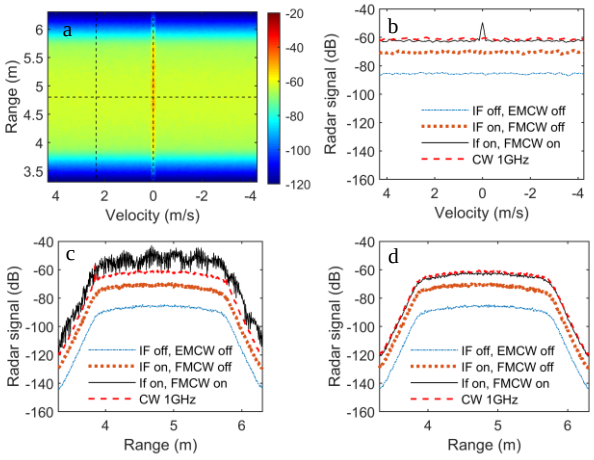

Fig. 4. Noise floor in the range Doppler map. (a) General view of the noise floor with the cuts that are presented in (b-d) indicated. (b) Constant range cut. (c) Constant velocity cut at 0-Doppler. (d) Constant velocity cut at finite Doppler. The traces in (b-d) are:

1. IF amplifiers off. Only ADC noise present
2. IF amplifiers on. Noise floor lifted ~10 dB above ADC noise
3. A cw LO signal at 10.1 GHz is applied to the Tranceiver input. Excess noise of ~8 dB is added
4. FMCW chirp is applied to the transceiver input. Exess noise (sidelobes) are seen in 0-Doppler.

in the subharmonic mixing that is worse than would be the case in a dedicated mixer and through excess AM noise from the LO (FMCW) drive that mix into the IF side of the transceiver (despite the balanced configuration). In addition, excess noise is generated in 0-Doppler from the process of driving the RF hardware with short (40 µs) chirps with high bandwidth. The cost of the excess noise is acceptable though, since S/N is in general sufficient in the application scenario that is evaluated.

Figure 5 shows how the noise floor for 0-Doppler and for finite Doppler is affected by the strength (RCS) of a static target (see section IV.A). The noise floor is calculated as the mean when averaging over relevant range bins within the IF filter bandwidth (excluding the range-bin with the target response). The noise floor in 0-Doppler is actually not random noise but the result of sidelobes and amplitude/phase modulation of the waveform, as well as multiple reflections in the RF hardware. At a finite Doppler frequency though, these effects are not seen since the sidelobe/modulation/reflection

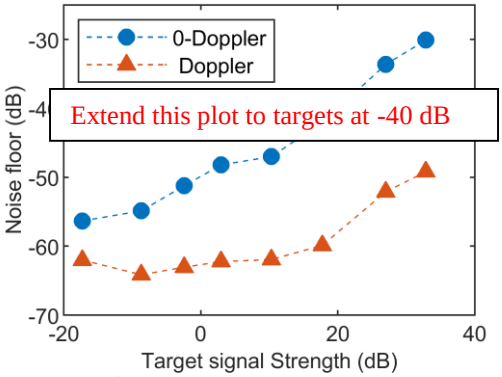

Fig. 5. The noise floor in 0-Doppler and Doppler dependent on target strength (RCS).

pattern is identical from pulse to pulse. At strong target returns, the noise floor increase also in Doppler, but then as a general increase of the noise floor in the whole range-Doppler plane - indicating that this noise floor originates in the actual noise of the RF carrier.

B. *Range resolution and small particle detection*

The target with three beads on a string was positioned so that all beads are illuminated by the radar beam, and angled so that the beads are separated in range by approximately 3 cm. The beads are clearly separated in the radar measurement and are visible with a S/N of approximately 20 dB (fig 6). When lightly tapping the string the beads are also separated in Doppler due to the fine Doppler resolution (0.06 m/s per Doppler bin).

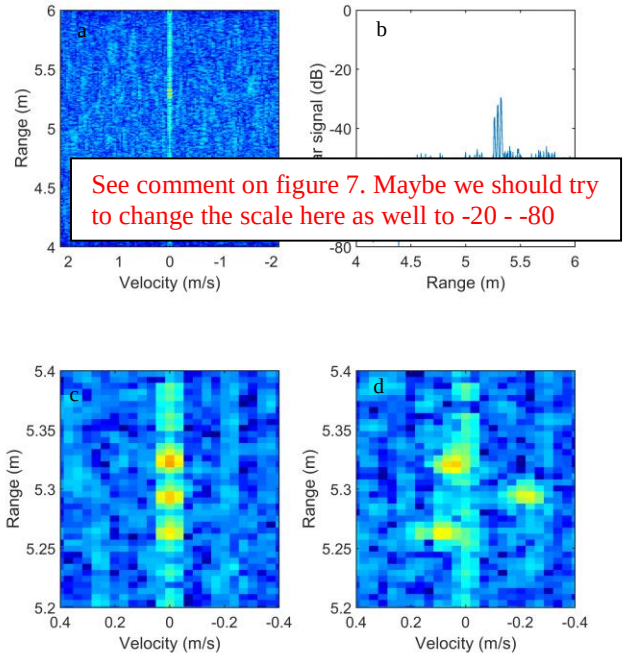

Fig 6 (a-c) shows a radar measurement of the three beads demonstrating that the beads are clearly resolved in range when positioned 3 cm apart in the range direction. The S/N is approximately 20 dB. (d)The string is vibrating, moving the beads in different directions resulting in small Doppler shifts for the beads.

In the demonstration of the capability to detect and follow small partilcles, small beads and grains of sand were dropped into the radar beam, that was folded to a vertical direction. 500 um diameter grains of quartz sand can be followed (including single grains) with significant S/N at 5 m distance (fig 7), proving the suitability of the radar instrument to monitor the dynamics of particle clouds. Experiments have been done with varying particle size – down to 75 um diameter with good results.

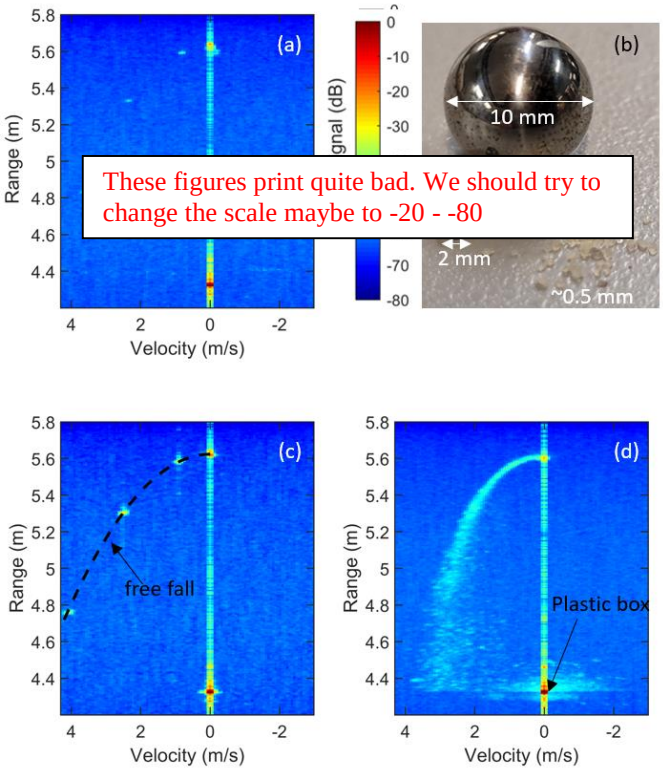

Fig. 7. Measurement of falling objects at 5 m distance. (a) shows the time integrated range-Doppler image of a 2 mm diameter falling metal bead. (b) shows the targets that are used in the experiments. (c) shows the time integrated range-Doppler image of the trajectory of a 10 mm diameter metal bead, together with the theoretical trajectory. (d) shows the time integrated range-Doppler image of a pinch of 500 um diameter quartz sand grains falling in the radar beam. At 4.4 m distance the grains hit the plastic box and bounce to a stop.

C. *Validation of velocity measurement*

Figure 7 (c) shows range-Doppler image of the free falling metal sphere integrated over several CPI. One can clearly see the acceleration of the metal sphere toward the radar. Each detection of the metal sphere corresponds to a separate CPI, or "frame", of the radar. Included in figure 7 (c) is also the theoretical trajectory from a free fall model. The measurement agrees very well with the theoretical free fall model, thus validating the velocity measurement of the radar.

VI. Conclusions

We have presented a 340 GHz frequency-modulated continuous-wave (FMCW) pulse-Doppler radar. The performance of the radar is described and it follows what is expected from theoretical predictions and the hardware specifications. The sensitivity of the instrument and the resolution, both in the spatial domain and in Doppler velocity, are adequate to map the dynamics of particle clouds.

Acknowledgment

The authors acknowledge funding from the Swedish foundation for strategic research (SSF).

References

Weather radars:
[Huber2009] M. Huber, and J. Trapp, "A review of NEXRAD Level II: Data, Distribution, and Applications," *The Journal of Terrestrial Observation*, vol. 1, no. 2, pp. 5–15, Spring 2009.

[Battaglia2014] A. Battaglia *et al.*, "G band atmospheric radars: new frontiers in cloud physics," *Atmos. Meas. Tech.*, vol. 7, no. 6, pp. 1527-1546, June 2014, DOI: 10.5194/amt-7-1527-2014.

[Kuechler2017] N. Küchler *et al.*, "A W-Band Radar–Radiometer System for Accurate and Continuous Monitoring of Clouds and Precipitation," *J. Atmos. Ocean. Tech.*, vol. 34, no. 11, pp. 2375-2392, Aug. 2017, DOI:10.1175/JTECH-D-17-0019.1.

[Durden2011] S. Durden *et al.* (2011, July). A cloud and precipitation radar system concept for the ACE Mission. Presented at IGRSS. Available: https://trs.jpl.nasa.gov/handle/2014/42129.

Automotive radars:
[Kärnfelt2009] C. Kärnfelt *et al.*, "77 GHz ACC radar simulation platform," in *ITST*, Lille, France, 2009, pp. 209-214, DOI: 10.1109/ITST.2009.5399354.

Books doppler radar processing:
[Parker2017] M. Parker, "Automotive Radar," in *Digital Signal Processing 101*, 2nd ed., Newnes, Elsevier, 2017, pp. 253-276, DOI: 10.1016/B978-0-12-811453-7.00020-2.

[Doviak1993] R. J. Doviak and D. S. Zrnić, "Doppler Spectra of Weather Signals," in *Doppler Radar and Weather Observations*, 2nd ed., Academic Press, 1993, pp. 87-121, DOI: 10.1016/B978-0-12-221422-6.50010-3.

[Bole2014] A. Bole, A. Wall, and A. Norris, "The Radar System – Technical Principles," in *Radar and ARPA Manual*, 3rd ed., Elsevier, 2014, ch. 2.9, pp. 29-137, DOI: 10.1016/B978-0-08-097752-2.00002-7.

340 GHz radars:
[Sheen2010] D. M. Sheen *et al.*, "Standoff concealed weapon detection using a 350-GHz radar imaging system," in *Proc. SPIE Defense, Security, and Sensing*, Orlando, Florida, United States, 2010, DOI: 10.1117/12.852788

[Cheng2018] B. Cheng *et al.*, "340-GHz 3-D Imaging Radar With 4Tx-16Rx MIMO Array," *IEEE T. THz Sci. Techn.*, vol. 8, no. 5, pp. 509-519, Sept. 2018, DOI: 10.1109/TTHZ.2018.2853551.

[Robertson2018] D. A. Robertson *et al.*, "A high frame rate, 340 GHz 3D imaging radar for security," in *RadarConf18*, Oklahoma City, OK, USA, 2018, pp. 0055-0060, DOI: 10.1109/RADAR.2018.8378530.

[Zamora2015] A. Zamora *et al.*, "A ×18 340 GHz InP HEMT multiplier chain," in *Proc. IMS*, Phoenix, AZ, USA, 2015, pp. 1-3, DOI: 10.1109/MWSYM.2015.7167009.

[Cooper2011] K. B. Cooper, R. J. Dengler, N. Llombart, B. Thomas, G. Chattopadhyay and P. H. Siegel, "THz Imaging Radar for Standoff Personnel Screening," *IEEE T. THz Sci. Tech.*, vol. 1, no. 1, pp. 169-182, Sept. 2011, DOI: 10.1109/TTHZ.2011.2159556.

600 GHz radar:

[Cooper2014] K. B. Cooper and G. Chattopadhyay, "Submillimeter-Wave Radar: Solid-State System Design and Applications," *IEEE Microw. Mag.*, vol. 15, no. 7, pp. 51-67, Nov.-Dec. 2014, DOI: 10.1109/MMM.2014.2356092.

90-170 GHz radars:
[Jaeschke2014] T. Jaeschke *et al.*, "High-Precision D-Band FMCW-Radar Sensor Based on a Wideband SiGe-Transceiver MMIC," *IEEE T. Microw. Theory.*, vol. 62, no. 12, pp. 3582-3597, Dec. 2014, DOI: 10.1109/TMTT.2014.2365460.

[Welp2020] B. Welp *et al.*, "Versatile Dual-Receiver 94-GHz FMCW Radar System With High Output Power and 26-GHz Tuning Range for High Distance Applications," *IEEE T. Microw. Theory.*, vol. 68, no. 3, pp. 1195-1211, March 2020, DOI: 10.1109/TMTT.2019.2955127.

220 – 340 GHz transceivers:
[Bryllert2013] T. Bryllert *et al.*, "Integrated 200–240-GHz FMCW Radar Transceiver Module," *IEEE T. Microw. Theory.*, vol. 61, no. 10, pp. 3808-3815, Oct. 2013, DOI: 10.1109/TMTT.2013.2279359.

[Dahlbäck2016] R. Dahlbäck *et al.*, "Compact 340 GHz homodyne transceiver modules for FMWC imaging radar arrays," *in Proc. IMS.*, San Francisco, CA, USA, 2016, pp. 1-4, DOI: 10.1109/MWSYM.2016.7540113.